Organic Electronics 99 (2021) 106327

Contents lists available at ScienceDirect

Organic Electronics

journal homepage: www.elsevier.com/locate/orgel

Controllable crystallization based on the aromatic ammonium additive for efficiently near-infrared perovskite light-emitting diodes

Chih-Chien Lee [a,1], Johan Iskandar [a,b,1], Abdul Khalik Akbar [b], Hsin-Ming Cheng [b,c,*], Shun-Wei Liu [b,c,**]

[a] Department of Electronic Engineering National Taiwan University of Science and Technology, Taipei City, 106335, Taiwan
[b] Organic Electronics Research Center, Ming Chi University of Technology, New Taipei City, 243303, Taiwan
[c] Department of Electronic Engineering, Ming Chi University of Technology, New Taipei City, 243303, Taiwan

ARTICLE INFO

Keywords:
Hybrid perovskite
Light-emitting diode
Near-infrared LEDs
Phenethylammonium iodide

ABSTRACT

Organic-inorganic hybrid perovskite have recently drawn appreciable attention for applications in light-emitting diodes (LEDs). However, the weak exciton binding energy of the methylammonium lead iodide perovskite introduces large exciton dissociation and low radiative recombination on its application as emission layer in near-infrared LEDs. Herein, we demonstrate the simple method by incorporating of phenethylammonium iodide (PEAI) into the perovskite can concurrently improve the radiative recombination rate for improving perovskite LED performances. Additionally, by introducing PEAI dramatically constrains the growth of perovskite crystals during film forming, producing crystallites with small dimensions, reducing roughness, and pin-hole free. After optimizing the emission layer in the perovskite LED, a high optical output power of 458.03 μW and external quantum efficiency of 5.25% are achieved, which represents a ~50-fold enhancement in the quantum efficiency compared to device without PEAI. Our work suggests a broad application prospect of perovskite materials for high optical output power LEDs and eventually a potential for solution-processed electrically pumped NIR laser diodes.

1. Introduction

The class of organic-inorganic hybrid perovskite has attracted a lot of attention due to their outstanding optical and electrical properties. High performance solar cell devices (SCs) with excellent power conversion efficiencies (>25%) and high-performance light emitting diodes (LEDs) have been reported recently [1–4]. Side by side with their impressive solar cells performance, perovskite materials exhibit strong photoluminescence (PL) properties and its emission color can be easily tuned by modifying the precursor solutions, making them very attractive candidate in the low-cost light emitting diodes and lasers. Particularly, $MAPbI_3$ ($MA = CH_3NH_3^+$) perovskites exhibit near infrared (NIR) emission with narrow spectra in the range of 740–800 nm, which makes them irresistible for prospective applications in night-vision devices, photodynamic therapeutics, security authentication technologies exploiting biometrics, and so on [5–8].

In the past few years, appreciable progress involving optimization of device structures and thin film depositions has been made in perovskite LEDs, especially the improvements in surface morphology, coverage rate, and crystal size of perovskite films due to they are the key factors influencing LED performance. Precisely controlling the growth conditions and parameters for perovskite films is the important way to pursue high quality perovskite LEDs and investigate its basic properties. Many treatment processes have been developed on improving the quality of the perovskite film including anti-solvent assisted one-step spin coating, two-step sequential deposition, and additive controlled crystallization [9–14]. An improved film quality and improved electrical properties were obtained by introducing non-ionic and dielectric polymers into perovskite. However, the performance of the devices showed an external quantum efficiency (EQE) of only below 1% [15].

Here, by simple method through introducing the bulky cation phenylethylammonium iodide ($PEAI = C_8H_{12}IN$) into perovskite precursors

* Corresponding author. Organic Electronics Research Center, Ming Chi University of Technology, New Taipei City, 243303, Taiwan.
** Corresponding author. Department of Electronic Engineering, Ming Chi University of Technology, New Taipei City, 243303, Taiwan.
E-mail addresses: cclee@mail.ntust.edu.tw (C. Lee), johan_iskandar@rocketmail.com (J. Iskandar), abdulkhalik96@gmail.com (A.K. Akbar), SMCheng@mail.mcut.edu.tw (H.-M. Cheng), swliu@mail.mcut.edu.tw (S. Liu).
[1] These authors contributed equally to this work.

https://doi.org/10.1016/j.orgel.2021.106327
Received 12 May 2021; Received in revised form 3 August 2021; Accepted 24 August 2021
Available online 27 August 2021

of methylammonium iodide (MAI) and lead iodide (PbI_2), we have obtained perovskite films with a controllable surface roughness and crystal size. This can happen because The PEAI molecules hindered crystal growth during crystal pinning and suppressed the exciton diffusion in the perovskite film [16]. Furthermore, the PEAI molecules passivated the exciton dissociation at crystal boundaries that reduced the recombination by trapping sites and enhanced the emission properties of the $MAPbI_3$ perovskite. In particular, the turn on voltage of perovskite LEDs decreased from 3.8 to 2.4 V followed by an increase in EQE and optical output power from 0.1 to 5.25% and 6.71 to 458.03 μW, respectively, which represents more than 50-fold enhancement in the quantum efficiency due to the incorporation of PEAI. The electroluminescence (EL) spectra of perovskite LED devices are matching to their corresponding PL spectra and remain stable at different bias voltages, which is crucial for practical LED applications.

2. Materials and methods

2.1. Materials

Methylammonium iodide (MAI, 99.99%) and Poly(*N*,*N*′-bis-4-butylphenyl-*N*,*N*′-bisphenyl)benzidine (Poly-TPD) were purchased from STAREK scientific Co., Ltd. Lead iodide (PbI_2, 99.99%) was purchased from Alfa aesar. Phenethyl ammonium iodide (PEAI, >99%) was purchased from Greatcell Solar Material Pty Ltd. 3′,3‴,3⁗-(1,3,5-triazine-2,4,6-triyl) tris(([1,1′-biphenyl]-3-carbonitrile (*C*N-T2T) was synthesized in the laboratory. Dimethyl sulfoxide (DMSO), *N*,*N*-dimethylformamide (DMF) and Chlorobenzene (CB) were purchased from Sigma-Aldrich. All the chemicals were used without further purification.

2.2. Film and device fabrication

ITO-coated glass substrates were cleaned successively with detergent, acetone and isopropanol, followed by drying and 20 min UV-ozone treatment. Poly-TPD was dissolved in chlorobenzene at a concentration of 8 mg mL–1. Poly-TPD was spin-coated on ITO at 1000 rpm. for 50 s, followed by thermal annealing at 150 °C for 10 min. The poly-TPD layer was treated by UV-ozone for 120 s to improve wetting before transfer into glovebox. The perovskite films were obtained from PEAI, MAI and PbI_2 blend solution in a binary solvent mixture of DMF and DMSO with a volume ratio of 4:1, then stirred at room temperature for overnight to attain clear light-yellow solution. The molar ratio of MAI:PbI_2 was fixed at 1:1 while varying the PEAI molar ratios in the powder blend (see details in Supplementary Table S4). Then, 50 μL perovskite precursor solution was deposited onto the substrates of ITO/poly-TPD with single step spin-coating procedure: 4000 rpm for 30 s, and the substrate was treated with 200 μL chlorobenzene after delay time of 10 s from the start of spinning. After thermal annealing and crystallization of the perovskite at 90 °C for 10 min, the perovskite films were post-treated with 100 μL phenethyl ammonium iodide solution (1 mg in 1 mL of isopropanol) using spin-coating method. Subsequently, LiF (1 nm), *C*N-T2T (60 nm), LiF (1.2 nm) and an Al (100 nm) anode were deposited by thermal evaporation under high vacuum (2×10^{-6} Torr). The active area of the devices was 4 mm^2.

2.3. Characterization and measurement of devices

X-ray diffraction was performed using a Bruker D8 Advance diffractometer employing Cu-Kα radiation. Scanning electron microscopy images were taken with a JEOL JSM-7610FPlus Field Emission Scanning Electron Microscope, while the surface roughness was performed using a Bruker Innova AFM. Steady-state absorption was carried out using a JASCO V-770 UV–visible spectrophotometer. Steady-state PL and time-resolved photoluminescence (TRPL) spectra were conducted with a HORIBA FluoroMax Plus. In the steady-state PL, the thin film sample was studied at an excitation wavelength of 305 nm using an ozone-free Xe arc lamp under ambient condition. In the TRPL measurement, all photo-luminescence decays were measured using a NanoLED pulsed diode controller HORIBA N-320 at an excitation wavelength of 320 nm with a pulse frequency of 50 kHz.

The perovskite LEDs were characterized after encapsulation using epoxy glue and a glass cover. The EL spectra and current-voltage-output power characteristics were measured in air using a Keysight Technologies B2901A Sourcemeter in conjunction with an EnliTech LQ-100R. The voltage range of 0–6 V was swept with an interval step of 0.2 V. The C–V characteristics were measured at a fixed frequency of 1 kHz with a voltage range of 0–5 V under dark conditions using an XM Solartron.

3. Results and discussion

XRD analysis was carried out to understand the effect of phenethylammonium iodide (PEAI) as an additive on the structural properties of the perovskite films. XRD patterns of the perovskite films prepared with different molar ratios of PEAI:$MAPbI_3$ are shown in Fig. 1a. Both perovskite films with and without PEAI show strong peaks at 14.2°, 28.2°, and 28.6°, which are corresponding to (110), (004) and (220) planes of tetragonal perovskite structure, respectively [17–19]. With increasing the concentration of PEAI in the perovskite films, the XRD peaks were slightly broadens, and slightly shifted toward higher angles, indicating that the lattice constant of $MAPbI_3$ is reduced, likely be due to the strain effect, which can be evidenced from the estimated microstrain value by using Wilson formula (Supplementary Equation 1) [20]. Microstrain in the corresponding perovskite films with and without PEAI is shown in Table S1 (Supplementary Information). As seen in Table S1, with PEAI, presents a higher microstrain compared to the without PEAI. We assume that the cation (phenthylammonium:PEA) incorporation results in increased microstrain due to the higher degree of lattice distortion [21]. This may occur because of the rearrangement of atoms in perovskite when incorporating PEAI, and this induces isotropic lattice shrinkage along multiple directions [22]. Moreover, the full-width at half-maximum (FWHM) of the diffraction peaks increases after adding PEAI (Fig. 1b), indicating that crystallite size decreases. The average crystallite sizes of the $MAPbI_3$ estimated from the prominent (110) facet by applying a Scherrer analysis on the assumption of spherical perovskite crystals are reducing from ~37 to ~27 nm for PEAI:$MAPbI_3$ loadings of 0:10 to 3:10, respectively (see details in Supplementary Table S1). At the moment we speculate that this is due to the inter-diffusion of the alkylammonium cation (PEA) into the perovskite, which affect the growth of perovskite crystals and quality of the film in finally [23]. These results confirm that our solution processing relying on the mixing of PEAI in the perovskite precursor can effectively reduce the size of the perovskite crystals. The smaller crystallite size can limit the exciton diffusion, which can improve the performance of the corresponding perovskite LED [15].

The absorption and PL spectra of perovskite films with different molar ratios of PEAI:$MAPbI_3$ in the precursor solution are shown in Fig. 1c. By adding the PEAI contents to the $MAPbI_3$ caused a narrowing in the band gap and caused an increase in the excitonic absorption peak (the details band gap in Supplementary Fig. S2). Increase in excitonic absorption intensity as the PEAI content increased may be due to the increase in the number of excitons. We assume that the increasing of the number of excitons dependent on the crystals dimension, where the excitonic absorption intensity can be increased with the reduction of size, in line with our findings from XRD as discussed previous. These results are in agreement with the reference [24]. In turn, the PL peaks of perovskite films gradually blue-shift with increasing PEAI content from 0:10 to 3:10. The blue-shifted PL emission is due to the reduced perovskite crystallite size, which is consistent with previous work by Xiao et al. Without being normalized, the PL intensity of the perovskite film increases consistently when the PEAI content increases (Supplementary Fig. S1). From the estimated PL lifetimes, it is observed that

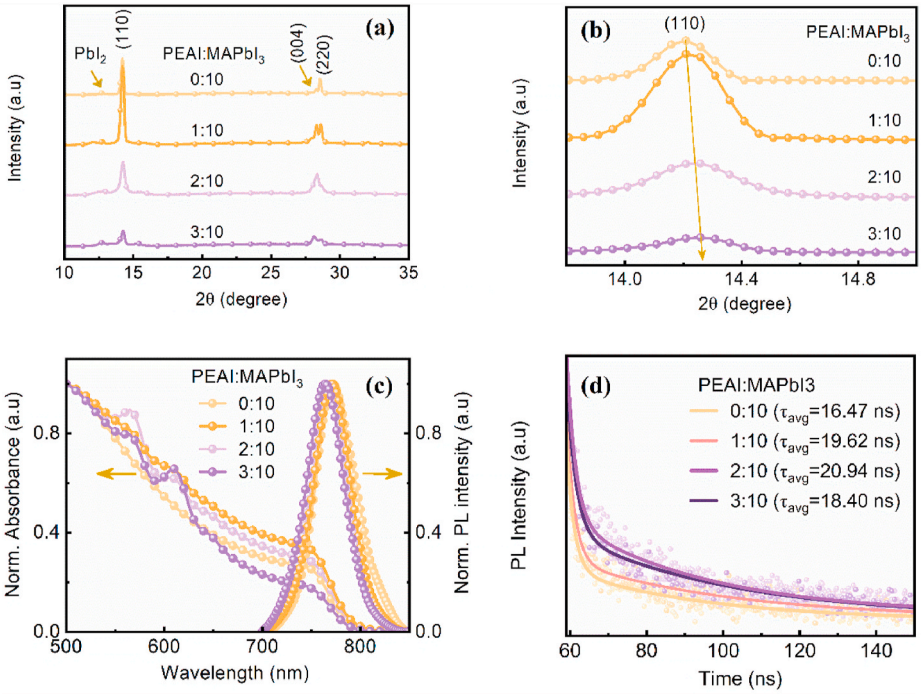

Fig. 1. Properties of perovskite films with different PEAI concentrations on quartz/poly-TPD substrates, (a) x-ray diffraction of all perovskite film, (b) enlarged XRD pattern of all perovskite film at (110) facet. (c) Normalized absorbance and photoluminescence spectra of all perovskite film (d) the TRPL decay curve of all perovskite film on glass/poly-TPD substrate.

with increasing the molar ratio of PEAI from 0:10 to 2:10, average decay time (τ_{avg}) gradually increases from 16.47 to 20.94 ns. Such a prolonged radiative lifetime and increased PL intensity indicate a gradual reduction of nonradiative recombination rates in perovskite film with the increasing PEAI content. This also demonstrates that the PEAI can prevent the excitons from diffusing into trapping sites located between perovskite crystal [15]. However, after increasing the PEAI molar ratio to 3:10, the PL intensity and τ_{avg} is slightly lower than that champion device, this may be due to the higher content of PEAI can hinders the electron generation and is detrimental to the performance of perovskite LED.

To further understand the morphology influence on the performance of perovskite LED, the atomic force microscope (AFM) images of perovskite films were obtained, as shown in Fig. 2. As the PEAI concentration increases, the $MAPbI_3$ films become smoother, with rms roughness of 15.4, 8.15, 6.54 and 7.81 nm for PEAI molar ratio of 0:10, 1:10, 2:10 and 3:10, respectively. The smoother surface could be attributable to the reduced mean free path of perovskite film, due to a decrease in the crystallite size and a shrink in the size distribution [25, 26]. The smooth surface of the perovskite layer is a crucial factor for perovskite LED since it can prevent the undesired electrical shunting path by direct contact of the perovskite layer and Al cathode, which can inhibit the recombination occurring at the perovskite/ETL interface and thus contribute to the enhancement of perovskite LED [27–29]. In

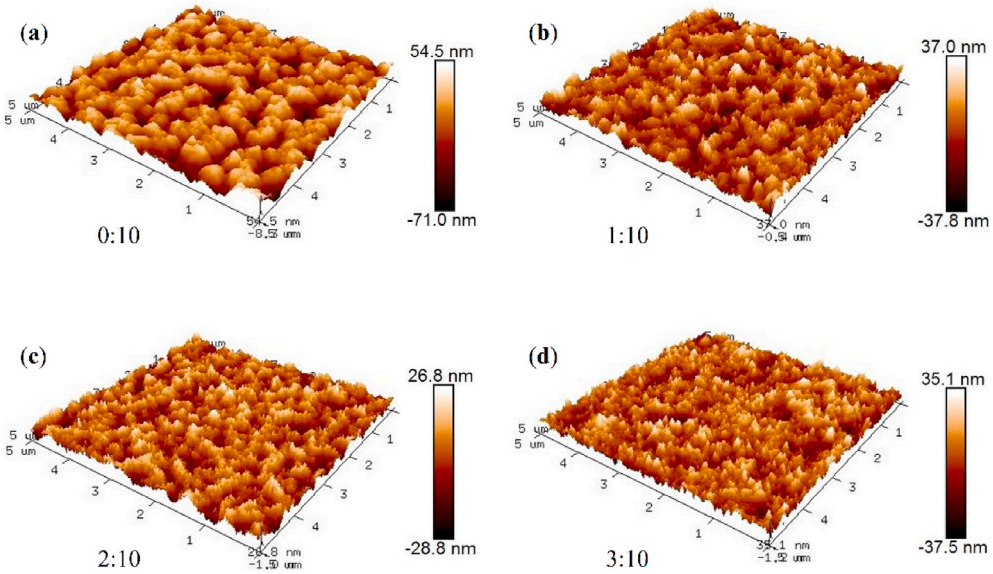

Fig. 2. AFM images of $PEAI:MAPbI_3$ film with molar ratio of (a) 0:10, (b) 1:10, (c) 2:10 and (d) 3:10.

agreement with the XRD and AFM results, the small crystallite size of the perovskite film after incorporation of PEAI is verified by scanning electron microscopy (SEM) (Supplementary Fig. S3). SEM images exhibits the morphology transformation of the perovskite film with the increasing PEAI content. In perovskite film without PEAI, it can be found that a number of large pin-holes are distributed, that will create electrical shunting paths and increase the leakage current. With increasing the PEAI concentration, these voids are may filled by the PEAI which results in pin-hole free thin films where the electrical shunting paths are reduced.

In our perovskite LED structure, we added a thin layer of LiF between perovskites and *CN*-T2T because it can improve the performance of the devices significantly (see details in Supplementary Table S2). As shown in Fig. 3a, a perovskite LED with the structure ITO/poly-TPD/perovskite/LiF/CN-T2T/LiF/Al was fabricated by solution processing. The perovskite and PEAI was used as the emission layer (EML) and additive, respectively. The other layers are typical constituents of a perovskite LED, poly-TPD [Poly(*N*,*N*′-bis-4-butylphenyl-*N*,*N*′-bisphenyl) benzidine], lithium fluoride (LiF), *CN*-T2T [3′,3‴,3⁗′′-(1,3,5-triazine-2,4,6-triyl)tris(([1,1′-biphenyl]-3-carbonitrile) act as the hole transport layer (HTL), interlayer, and electron transport layer (ETL), respectively, while ITO and LiF/Al are the anode and cathode, respectively. In this study we used the unpopular ETL *CN*-T2T instead of the common ETL TPBi (the molecular structures illustrated in Supplementary Fig. S5). All energy level values (in Fig. 3b) are from the literature [30–34]. In this section we add the spectrum of absorbance and photoluminescence of the perovskite solution to further study the effect of PEAI on the perovskite precursor. In Fig. 3d, the absorption spectrum of the perovskite solutions with and without PEAI exhibits different features than the thin films, with no exciton peaks clearly observed. The photoluminescence spectrum of the perovskite solution with and without PEAI shows a similar peak at 763 nm. The intensity of photoluminescence spectra of the perovskite solution increase with introducing PEAI, which is in agreement with perovskite thin film. Fig. 3c shows the photograph of perovskite LED at an operating voltage of 4 V. Perovskite LED with PEAI exhibits uniform and bright emission compared to the device without PEAI. This is similar to that shown by the EL spectra which will be discussed in the next section.

The EL spectra of the perovskite LEDs are shown in Fig. 4a, together with a normalized EL spectra (inset) are affixed to clearly observe and compare the changes of light emission of the devices with different PEAI concentrations. A gradual blue shift of EL from 767 to 756 nm was observed as the PEAI ratio increased (see Table 1), which correlated well with the blue shift of PL spectra due to the decreasing in bandgap (Supplementary Fig. S2). This phenomenon is in good agreement to that observed in the energy level tuning in colloidal quantum dot by Jasieniak et al. [35]. With the blue shift of EL spectra, the corresponding Commission Internationale de l'Eclairage (CIE) value also changed from (0.709, 0.290) to (0.725, 0.274) as shown in Fig. 4b and Table 1. These coordinates are close to the red-NIR emission coordinate in previous finding by OLED group [36]. In addition, without being normalized, the EL of perovskite LEDs with molar ratio of 0:10 has the weakest integrated EL intensity and becomes stronger with increasing additive concentration. However, when the molar ratio is increased to 3:10, the EL performance starts to deteriorate. It may be attributed to the fact that the direct charge carrier well-captured at low additive concentrations. This occurrence indicates that direct charge carrier trapping at the PEAI molecule has a substantial position to the energy transfer in the devices and that charge carrier trapping process is significant in perovskite LED with molar ratio of 2:10 [37].

The current density–voltage–output power (J–V–P) curves and corresponding external quantum efficiency (EQE) curves are shown in Fig. 4c and d, respectively. We can see that the perovskite LED with molar ratio of 0:10 possesses the highest current density compared with the other three devices at low applied voltages (<1.5 V). The larger current in the device relevant to the shunt paths due to the incomplete surface coverage or pinholes, which is consistent with the SEM image (Supplementary Fig. S3a), thereby resulting in poor EL emission and EQE is 0.1% for device without PEAI. This may be due to the high number of non-radiative recombination in perovskite film, leading to its higher V_{on} than perovskite film with PEAI [38]. On the contrary, the lower pinholes in perovskite film contains PEAI, the EQE of the perovskite LEDs increased to 5.25% for molar ratio of 2:10. Moreover, in Fig. 4d shows when the EQE reaches a maximum value, the value is relatively stable at higher voltages for all perovskite LEDs with PEAI, indicating that excellent stability compare with the perovskite LED without PEAI. We propose this result is attributable to either of two causes: (1) the existence of PEAI reduces the joule heating or (2) more

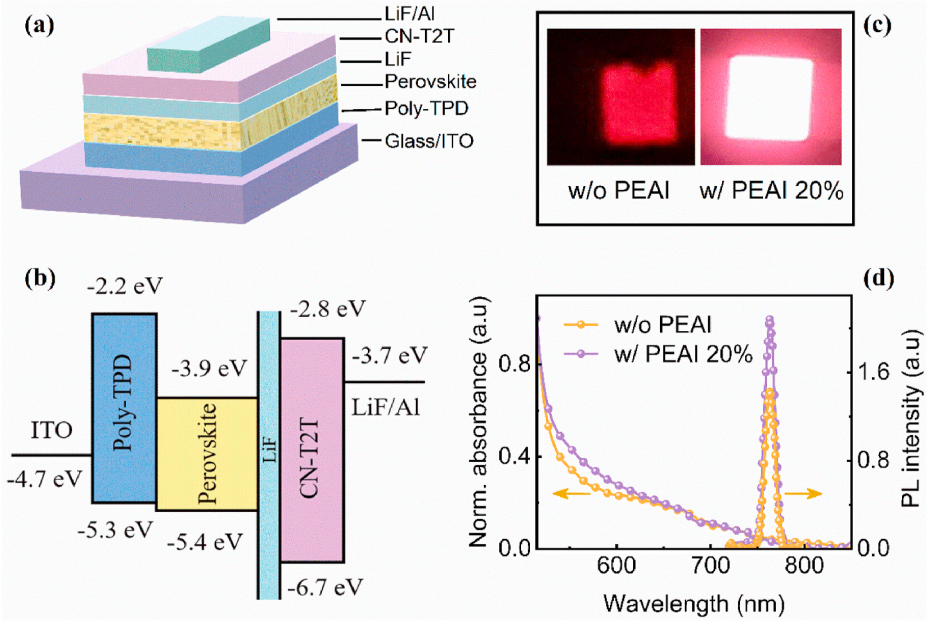

Fig. 3. (a) Device structure of perovskite LED, (b) energy level diagram of perovskite LED, (c) real photograph of perovskite LED, (d) normalized absorbance and PL spectra of perovskite solution.

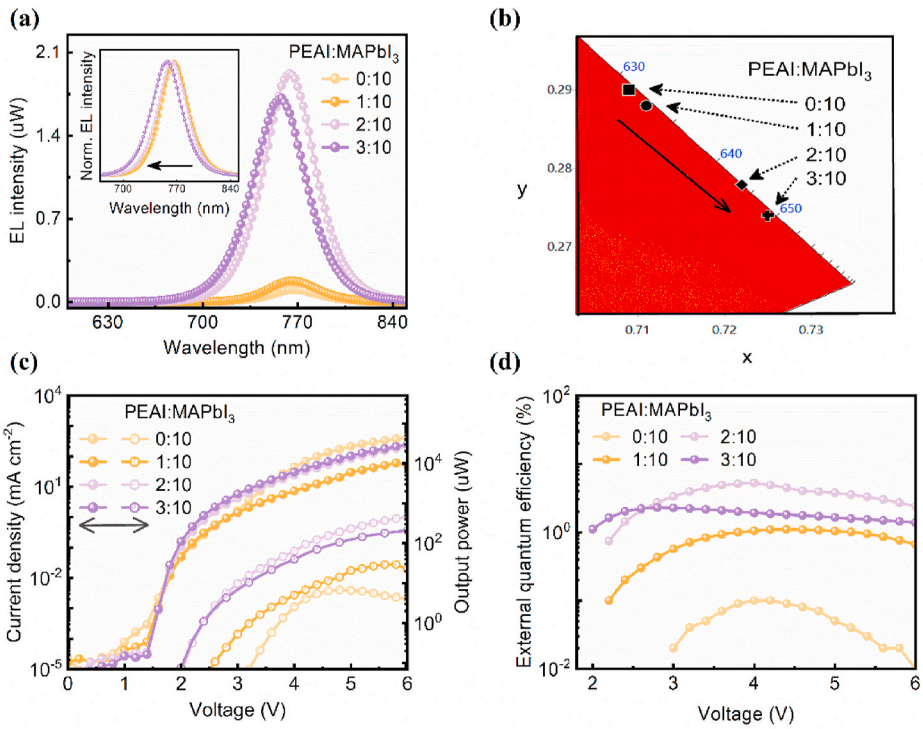

Fig. 4. The performance of perovskite LEDs with different PEAI ratios (a) electroluminescence spectra, (b) Commission Internationale de l'Eclairage (CIE) values of the EL spectra (c) voltage – output power – current density plots (d) external quantum efficiency.

Table 1
Summary of device performance with different molar ratios of PEAI.

PEAI: $MAPbI_3$	PL/EL peak (nm)	V_{on} (V)	P_{max} (uW)	EQE_{max} (%)	CIE (x, y)
0:10	772/767	3.8	6.71	0.1	(0.709, 0.290)
1:10	771/766	3.2	29.28	1.1	(0.711, 0.289)
2:10	770/764	2.4	458.03	5.25	(0.722, 0.277)
3:10	764/756	2.4	206.72	2.29	(0.725, 0.274)

Turn-on voltage V_{on}, maximum output power P_{max}, maximum external quantum efficiency EQE_{max}, Commission Internationale de l'Eclairage CIE.

balanced charge injection derived from improved current efficiency (Supplementary Fig. S4a) [15,39]. For comparison, we have fabricated the devices using common ETL TPBi, we obtained that the highest EQE of 3.10% owned by perovskite LED 2:10 (see details in Supplementary Fig. S6 and Table S3).

Apart from the impressive EQE, to our greater surprise is the reduction of turn-on voltage (V_{on}) and outstanding improvement of maximum output power (P_{max}). The perovskite LED with molar ratio of 0:10 has a turn-on voltage of 3.8 V (defined as the voltage at which output power of 1 μW was measured) and a maximum output power of 6.71 μW. After employing the PEAI as additive, the device has an obviously reduced turn-voltage of 2.4 V and maximum output power of 458.03 μW for devices with molar ratio of 2:10. We suggest that the improved performance of perovskite LEDs may originate from the improvement of perovskite film quality because of the existence of PEAI as discussed earlier, thus significantly demoted the V_{on} and elevated the P_{max}.

For a multi-layered perovskite LED structure, radiative recombination processes might happen at the interfaces, which commonly alter the EL spectrum and restrict device performances. As observed in Supplementary Fig. S4b, stable and bright EL spectra from the perovskite LED under different biases demonstrate that unwanted radiative recombination pathways are effectively removed. As a result, strong EL signals without any additional peaks are obtained, which is crucial for practical LED applications. The luminance and power conversion efficiency (PCE) curves of perovskite LEDs are shown in Supplementary Figs. S4c and S4d, respectively. The peak luminance and PCE of the devices are relatively low due to the near-infrared light emission.

The capacitance–voltage (C–V) analysis is one of the most efficient methods to evaluate the electronic properties of the perovskite LEDs [40]. The C–V characteristics were measured at a fixed frequency of 1000 Hz under dark conditions. Fig. 5 shows the C–V characteristics of the four devices, we divide the C–V curves into three regions, (I) below

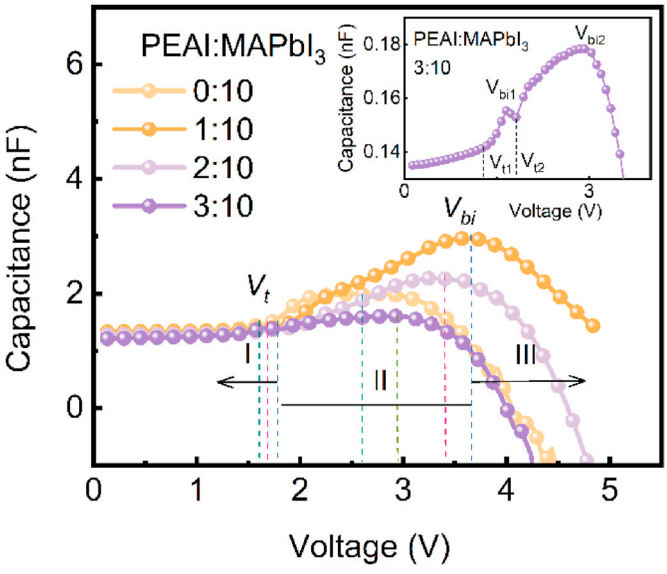

Fig. 5. Capacitance–voltage curve of perovskite LEDs with different PEAI ratios.

threshold voltage (V_t), (II) within V_t and built-in voltage (V_{bi}) and (III) above V_{bi}. In region I, no charge recombination or light emission was observed for all devices. In other words, charges are not injected into the perovskite layers because at this region only the charge process occurs at both electrodes ITO and Al [32,41]. Therefore, at this region there is no significant difference in their capacitance values due to similar electrode parameters and materials. An incisive capacitance increases in region II, the capacitances of all of the devices start rising with the increase of bias voltage, which corresponds to the charge injection and diffusion in the transport layer [42,43]. As a consequence, a peak in the voltage dependence of the capacitance is created. Furthermore, we observe the capacitance peak in perovskite LED with molar ratio of 0:10 is stable at 2 nF, from a voltage of 2–3 V, indicating that no recombination is occurring at this range, likely be due to the charge-carrier trapping [44]. From our point of view, the possibly reason is prior to the arrival of subsequent supplied voltage (>3 V), carriers will remain as trapped charge-carrier until the commencement of the next excitation cycle, then a light begin to be emitted [45,46]. For the device with molar ratio of 1:10, the peak capacitance further increases to 3 nF which indicate the significant charge accumulation owing inefficient charge transport, by way of explanation, the carrier's injection rate is faster than the consumption rate [47]. In contrast, perovskite LED with molar ratio of 2:10 exhibits balance charge injection and recombination thus lead a significant improvement to its performance. To support our argument, in (Supplementary Fig. S1) we compare the PL intensity for all devices that can be attributed to the recombination rate in the active layer. The PL intensity of perovskite film with molar ratio of 2:10 is higher than other three devices, the high PL intensity of the device corresponds to the high recombination rate of electrons and holes [48]. However, when the additive ratio enlarges to 3:10, the *C*–V curve showed a very weak increase.

Thus, we speculate that one of the main reasons for the weak increase in capacitance is carriers may possibly head across the device without trapping, following in little contribution to capacitance [49]. Furthermore, there are two peaks appear for perovskite LED with molar ratio of 3:10 as depicted in Fig. 5 inset. The minor and major peaks appear which refers to the injection of charges into the device. At the minor peak, the capacitance increases at threshold voltage V_{t1} (1.35 V) due to the injection of holes, where at built-in voltage V_{bi1} (1.65 V) some electrons can be injected. Hereinafter, the capacitance decreases until the threshold voltage V_{t2} of the major peak. For the major peak, holes are injected into the poly-TPD layer at V_{t2} (1.81 V) later at V_{bi2} (3.03 V), electrons start to inject from the cathode into the device. Henceforward, electrons and holes recombine to emit the light. In region III, the bias at which capacitance starts to decrease sharply marks the occurrence of efficient radiative recombination. In other words, the electron-hole pairs annihilate each other which causes a decrease in capacitance and get negative at certain bias voltage. The negative capacitances can be caused by self-heating or over injection of charge carriers into the perovskite layer, leading to an enhanced nonradiative recombination [50,51].

4. Conclusions

In summary, we demonstrate that the crystallite size of the perovskite can be decreased to about 20–30 nm by introducing the PEAI into $MAPbI_3$ perovskite precursors. With the control of the crystallite size, we experimentally proved the enhancement in the charge recombination in the perovskite films thus resulting more efficient radiative rate by suppression of the exciton diffusion. Meanwhile, the pin-hole free perovskite film with the surface roughness greatly reduced approximately by 40% compared to perovskite films without PEAI is realized. The reduction of the pin-holes and surface roughness of the perovskite films reduces the leakage current and facilitates the formation of films on top that aids the device fabrication. As a direct result, the optimized NIR perovskite LED with molar ratio of 2:10 exhibited a high optical output power (458.03 μW) and an EQE of 5.25%, which represents a ~50-fold increment in the quantum efficiency compared to the control device with molar ratio of 0:10. The concept can be applied in visible LEDs and laser by adjusting the composition of the perovskites.

Author contributions

Hsin-Ming Cheng: Conceptualization, Methodology, Resources, Writing-Review & Editing, Validation, Funding acquisition. **Johan Iskandar**: Methodology, Data curation, Investigation, Formal analysis, Writing-Original draft. **Abdul Khalik Akbar**: Data curation, Investigation. **Chih-Chien Lee**: Supervision, Funding acquisition. **Shun-Wei Liu**: Resources, Supervision, Project administration, Funding acquisition.

Declaration of competing interest

The authors declare that they have no known competing financial interests or personal relationships that could have appeared to influence the work reported in this paper.

Acknowledgements

We acknowledge the Ministry of Science and Technology, Taiwan (Grant Nos. MOST 109-2112-*M*-131-001, 109-2223-E-131-001-MY3 and 109-2221-E-011-156) for the financial support.

Appendix A. Supplementary data

Supplementary data to this article can be found online at https://doi.org/10.1016/j.orgel.2021.106327.

References

[1] National Renewable Energy Laboratory. https://www.nrel.gov/pv/assets/pdfs/best-research-cell-efficiencies.20190802.pdf. (Accessed 24 March 2021).
[2] Z. Ren, J. Yu, Z. Qin, J. Wang, J. Sun, C.C.S. Chan, S. Ding, K. Wang, R. Chen, K. S. Wong, et al., High-performance blue perovskite light-emitting diodes enabled by efficient energy transfer between coupled quasi-2D perovskite layers, Adv. Mater. 33 (2021) 1–10, https://doi.org/10.1002/adma.202005570.
[3] K. Lin, J. Xing, L.N. Quan, F.P.G. de Arquer, X. Gong, J. Lu, L. Xie, W. Zhao, D. Zhang, C. Yan, et al., Perovskite light-emitting diodes with external quantum efficiency exceeding 20 per cent, Nature 562 (2018) 245–248, https://doi.org/10.1038/s41586-018-0575-3.
[4] A. Giuri, Z. Yuan, Y. Miao, J. Wang, F. Gao, N. Sestu, M. Saba, G. Bongiovanni, S. Colella, C. Esposito Corcione, et al., Ultra-bright near-infrared perovskite light-emitting diodes with reduced efficiency roll-off, Sci. Rep. 8 (2018) 1–8, https://doi.org/10.1038/s41598-018-33729-9.
[5] L. Yao, S. Zhang, R. Wang, W. Li, F. Shen, B. Yang, Y. Ma, Highly efficient near-infrared organic light-emitting diode based on a butterfly-shaped donor-acceptor chromophore with strong solid-state fluorescence and a large proportion of radiative excitons, Angew. Chem. 126 (2014) 2151–2155, https://doi.org/10.1002/ange.201308486.
[6] L. Maggini, I. Cabrera, A. Ruiz-Carretero, E.A. Prasetyanto, E. Robinet, L. De Cola, Breakable mesoporous silica nanoparticles for targeted drug delivery, Nanoscale 8 (2016) 7240–7247, https://doi.org/10.1039/c5nr09112h.
[7] X.B. Han, H.X. Li, Y.Q. Jiang, H. Wang, X.S. Li, J.Y. Kou, Y.H. Zheng, Z.N. Liu, H. Li, J. Li, et al., Upconversion nanoparticle-mediated photodynamic therapy induces autophagy and cholesterol efflux of macrophage-derived foam cells via ROS generation, Cell Death Dis. 8 (2017), e2864, https://doi.org/10.1038/cddis.2017.242.
[8] A. Zampetti, A. Minotto, F. Cacialli, Near-infrared (NIR) organic light-emitting diodes (OLEDs): challenges and opportunities, Adv. Funct. Mater. 29 (2019) 1–22, https://doi.org/10.1002/adfm.201807623.
[9] Y.J. Kang, S.N. Kwon, S.P. Cho, Y.H. Seo, M.J. Choi, S.S. Kim, S.I. Na, Antisolvent additive engineering containing dual-function additive for triple-cation p-i-n perovskite solar cells with over 20% PCE, ACS Energy Lett 5 (2020) 2535–2545, https://doi.org/10.1021/acsenergylett.0c01130.
[10] C.H. Chiang, J.W. Lin, C.G. Wu, One-step fabrication of a mixed-halide perovskite film for a high-efficiency inverted solar cell and module, J. Mater. Chem. 4 (2016) 13525–13533, https://doi.org/10.1039/c6ta05209f.
[11] D. Bi, S.J. Moon, L. Häggman, G. Boschloo, L. Yang, E.M.J. Johansson, M. K. Nazeeruddin, M. Grätzel, A. Hagfeldt, Using a two-step deposition technique to prepare perovskite (CH 3NH3PbI3) for thin film solar cells based on ZrO2 and TiO2 mesostructures, RSC Adv. 3 (2013) 18762–18766, https://doi.org/10.1039/c3ra43228a.

[12] J. Wu, X. Xu, Y. Zhao, J. Shi, Y. Xu, Y. Luo, D. Li, H. Wu, Q. Meng, DMF as an additive in a two-step spin-coating method for 20% conversion efficiency in perovskite solar cells, ACS Appl. Mater. Interfaces 9 (2017) 26937–26947, https://doi.org/10.1021/acsami.7b08504.
[13] Y. Zhou, Z. Zhou, M. Chen, Y. Zong, J. Huang, S. Pang, N.P. Padture, Doping and alloying for improved perovskite solar cells, J. Mater. Chem. 4 (2016) 17623–17635, https://doi.org/10.1039/C6TA08699C.
[14] T. Li, Y. Pan, Z. Wang, Y. Xia, Y. Chen, W. Huang, Additive engineering for highly efficient organic-inorganic halide perovskite solar cells: recent advances and perspectives, J. Mater. Chem. 5 (2017) 12602–12652, https://doi.org/10.1039/c7ta01798g.
[15] H. Lin, L. Zhu, H. Huang, C.J. Reckmeier, C. Liang, A.L. Rogach, W.C.H. Choy, Efficient near-infrared light-emitting diodes based on organometallic halide perovskite-poly(2-ethyl-2-oxazoline) nanocomposite thin films, Nanoscale 8 (2016) 19846–19852, https://doi.org/10.1039/c6nr08195a.
[16] H. Cho, S.H. Jeong, M.H. Park, Y.H. Kim, C. Wolf, C.L. Lee, J.H. Heo, A. Sadhanala, N.S. Myoung, S. Yoo, et al., Overcoming the electroluminescence efficiency limitations of perovskite light-emitting diodes, Science 350 (2015) 1222–1225, https://doi.org/10.1126/science.aad1818 (80-.).
[17] C.M. Tsai, G.W. Wu, S. Narra, H.M. Chang, N. Mohanta, H.P. Wu, C.L. Wang, E.W. G. Diau, Control of preferred orientation with slow crystallization for carbon-based mesoscopic perovskite solar cells attaining efficiency 15%, J. Mater. Chem. 5 (2017) 739–747, https://doi.org/10.1039/c6ta09036b.
[18] S. Kavadiya, J. Strzalka, D.M. Niedzwiedzki, P. Biswas, Crystal reorientation in methylammonium lead iodide perovskite thin film with thermal annealing, J. Mater. Chem. 7 (2019) 12790–12799, https://doi.org/10.1039/c9ta02358e.
[19] T. Oku, Crystal structures of CH3NH3PbI3 and related perovskite compounds used for solar cells, Sol. Cells - New Approaches Rev. (2015), https://doi.org/10.5772/59284.
[20] R. Rai, T. Triloki, B.K. Singh, X-ray diffraction line profile analysis of KBr thin films, Appl. Phys. Mater. Sci. Process 122 (2016) 1–11, https://doi.org/10.1007/s00339-016-0293-3.
[21] G. Zheng, C. Zhu, J. Ma, X. Zhang, G. Tang, R. Li, Y. Chen, L. Li, J. Hu, J. Hong, et al., Manipulation of facet orientation in hybrid perovskite polycrystalline films by cation cascade, Nat. Commun. 9 (2018) 1–11, https://doi.org/10.1038/s41467-018-05076-w.
[22] S. Zhang, S. Wu, R. Chen, W. Chen, Y. Huang, H. Zhu, Z. Yang, W. Chen, Controlling orientation diversity of mixed ion perovskites: reduced crystal microstrain and improved structural stability, J. Phys. Chem. Lett. 10 (2019) 2898–2903, https://doi.org/10.1021/acs.jpclett.9b01180.
[23] T.M. Koh, V. Shanmugam, X. Guo, S.S. Lim, O. Filonik, E.M. Herzig, P. Müller-Buschbaum, V. Swamy, S.T. Chien, S.G. Mhaisalkar, et al., Enhancing moisture tolerance in efficient hybrid 3D/2D perovskite photovoltaics, J. Mater. Chem. 6 (2018) 2122–2128, https://doi.org/10.1039/c7ta09657g.
[24] Z. Xiao, R.A. Kerner, L. Zhao, N.L. Tran, K.M. Lee, T.W. Koh, G.D. Scholes, B. P. Rand, Efficient perovskite light-emitting diodes featuring nanometre-sized crystallites, Nat. Photonics 11 (2017) 108–115, https://doi.org/10.1038/nphoton.2016.269.
[25] X. Yang, H. Gu, S. Li, J. Li, H. Shi, J. Zhang, N. Liu, Z. Liao, W. Xu, Y. Tan, Improved photoelectric performance of all-inorganic perovskite through different additives for green light-emitting diodes, RSC Adv. 9 (2019) 34506–34511, https://doi.org/10.1039/c9ra05053a.
[26] C.Y. Huang, S.P. Chang, A.G. Ansay, Z.H. Wang, C.C. Yang, Ambient-processed, additive-assisted CsPbBr3 perovskite light-emitting diodes with colloidal NiOx nanoparticles for efficient hole transporting, Coatings 10 (2020), https://doi.org/10.3390/coatings10040336.
[27] C.Y. Chang, C.Y. Chu, Y.C. Huang, C.W. Huang, S.Y. Chang, C.A. Chen, C.Y. Chao, W.F. Su, Tuning perovskite morphology by polymer additive for high efficiency solar cell, ACS Appl. Mater. Interfaces 7 (2015) 4955–4961, https://doi.org/10.1021/acsami.5b00052.
[28] D.D.S. Fung, L. Qiao, W.C.H. Choy, C. Wang, W.E.I. Sha, F. Xie, S. He, Optical and electrical properties of efficiency enhanced polymer solar cells with Au nanoparticles in a PEDOT-PSS layer, J. Mater. Chem. 21 (2011) 16349–16356, https://doi.org/10.1039/c1jm12820e.
[29] Q.Q. Ge, J. Ding, J. Liu, J.Y. Ma, Y.X. Chen, X.X. Gao, L.J. Wan, J.S. Hu, Promoting crystalline grain growth and healing pinholes by water vapor modulated post-annealing for enhancing the efficiency of planar perovskite solar cells, J. Mater. Chem. 4 (2016) 13458–13467, https://doi.org/10.1039/c6ta05288f.
[30] J.M. Kim, C.H. Lee, J.J. Kim, Mobility balance in the light-emitting layer governs the polaron accumulation and operational stability of organic light-emitting diodes, Appl. Phys. Lett. 111 (2017) 2–7, https://doi.org/10.1063/1.5004623.
[31] C. Zhang, W. Luan, Y. Yin, High efficient planar-heterojunction perovskite solar cell based on two-step deposition process, Energy Procedia 105 (2017) 793–798, https://doi.org/10.1016/j.egypro.2017.03.391.
[32] N.R. Al Amin, K.K. Kesavan, S. Biring, C.-C. Lee, T.-H. Yeh, T.-Y. Ko, S.-W. Liu, K.-T. Wong, A comparative study via photophysical and electrical characterizations on interfacial and bulk exciplex-forming systems for efficient organic light-emitting diodes, ACS Appl. Electron. Mater. 2 (2020) 1011–1019, https://doi.org/10.1021/acsaelm.0c00062.
[33] C.Y. Chang, W.L. Hong, P.H. Lo, T.H. Wen, S.F. Horng, C.L. Hsu, Y.C. Chao, Perovskite white light-emitting diodes with a perovskite emissive layer blended with rhodamine 6G, J. Mater. Chem. C 8 (2020) 12951–12958, https://doi.org/10.1039/d0tc02471f.
[34] X. Liang, R.W. Baker, K. Wu, W. Deng, D. Ferdani, P.S. Kubiak, F. Marken, L. Torrente-Murciano, P.J. Cameron, Continuous low temperature synthesis of MAPbX3 perovskite nanocrystals in a flow reactor, React. Chem. Eng. 3 (2018) 640–644, https://doi.org/10.1039/c8re00098k.
[35] J. Jasieniak, M. Califano, S.E. Watkins, Size-dependent valence and conduction band-edge energies of semiconductor nanocrystals, ACS Nano 5 (2011) 5888–5902, https://doi.org/10.1021/nn201681s.
[36] C.L. Ho, H. Li, W.Y. Wong, Red to near-infrared organometallic phosphorescent dyes for OLED applications, J. Organomet. Chem. 751 (2014) 261–285, https://doi.org/10.1016/j.jorganchem.2013.09.035.
[37] G.W. Kang, Y.J. Ahn, C.H. Lee, Effects of doping in organic electroluminescent devices doped with a fluorescent dye, J. Inf. Disp. 2 (2001) 1–5, https://doi.org/10.1080/15980316.2001.9651859.
[38] Z.-L. Tseng, S.-H. Lin, J.-F. Tang, Y.-C. Huang, H.-C. Cheng, W.-L. Huang, Y.-T. Lee, L.-C. Chen, Polymeric hole transport materials for red CsPbI3 perovskite quantum-dot light-emitting diodes, Polymers 13 (2021) 896, https://doi.org/10.3390/polym13060896.
[39] C. Zou, Y. Liu, D.S. Ginger, L.Y. Lin, Suppressing efficiency roll-off at high current densities for ultra-bright green perovskite light-emitting diodes, ACS Nano 14 (2020) 6076–6086, https://doi.org/10.1021/acsnano.0c01817.
[40] S. Chen, W. Cao, T. Liu, S.W. Tsang, Y. Yang, X. Yan, L. Qian, On the degradation mechanisms of quantum-dot light-emitting diodes, Nat. Commun. 10 (2019) 1–9, https://doi.org/10.1038/s41467-019-08749-2.
[41] L. Zhang, H. Nakanotani, C. Adachi, Capacitance-voltage characteristics of a 4,4′-bis[(N-carbazole) styryl]biphenyl based organic light-emitting diode: implications for characteristic times and their distribution, Appl. Phys. Lett. 103 (2013) 8–12, https://doi.org/10.1063/1.4819436.
[42] A.A. Pil'nik, A.A. Chernov, D.R. Islamov, Charge transport mechanism in dielectrics: drift and diffusion of trapped charge carriers, Sci. Rep. 10 (2020) 1–10, https://doi.org/10.1038/s41598-020-72615-1.
[43] M.S. Al-Qrinawi, T.M. El-Agez, M.S. Abdel-Latif, S.A. Taya, Influence of copper phthalocyanine (CuPc) thin layer on capacitance-voltage characterization of a device consisting of ITO/CuPc/PVK/rhodamine B dye layers, Int. J. Thin Film. Sci. Technol. 6 (2017) 61–66, https://doi.org/10.18576/ijtfst/060202.
[44] J.E. Moser, Perovskite photovoltaics: slow recombination unveiled, Nat. Mater. 16 (2016) 4–6, https://doi.org/10.1038/nmat4796.
[45] R. Qian, H. Zong, J. Schneider, G. Zhou, T. Zhao, Y. Li, J. Yang, D.W. Bahnemann, J.H. Pan, Charge carrier trapping, recombination and transfer during TiO2 photocatalysis: an overview, Catal. Today 335 (2019) 78–90, https://doi.org/10.1016/j.cattod.2018.10.053.
[46] H.F. Haneef, A.M. Zeidell, O.D. Jurchescu, Charge carrier traps in organic semiconductors: a review on the underlying physics and impact on electronic devices, J. Mater. Chem. C 8 (2020) 759–787, https://doi.org/10.1039/c9tc05695e.
[47] M. Guan, L. Niu, Y. Zhang, X. Liu, Y. Li, Y. Zeng, Space charges and negative capacitance effect in organic light-emitting diodes by transient current response analysis, RSC Adv. 7 (2017) 50598–50602, https://doi.org/10.1039/c7ra07311a.
[48] Y. Zheng, L. Zheng, Y. Zhan, X. Lin, Q. Zheng, K. Wei, Ag/ZnO heterostructure nanocrystals: synthesis, characterization, and photocatalysis, Inorg. Chem. 46 (2007) 6980–6986, https://doi.org/10.1021/ic700688f.
[49] L. Zhang, D. Taguchi, T. Manaka, M. Iwamoto, Direct probing of the selective electron and hole accumulation at organic/organic interfaces in a triple-layer organic device by time-resolved optical second harmonic generation, Appl. Phys. Lett. 99 (2011) 2009–2012, https://doi.org/10.1063/1.3626851.
[50] E. Knapp, B. Ruhstaller, Analysis of negative capacitance and self-heating in organic semiconductor devices, J. Appl. Phys. 117 (2015) 135501, https://doi.org/10.1063/1.4916981.
[51] C. Blauth, P. Mulvaney, T. Hirai, Negative capacitance as a diagnostic tool for recombination in purple quantum dot LEDs, J. Appl. Phys. 125 (2019), https://doi.org/10.1063/1.5088177.